PCCP

Accepted Manuscript

This is an *Accepted Manuscript*, which has been through the Royal Society of Chemistry peer review process and has been accepted for publication.

Accepted Manuscripts are published online shortly after acceptance, before technical editing, formatting and proof reading. Using this free service, authors can make their results available to the community, in citable form, before we publish the edited article. We will replace this *Accepted Manuscript* with the edited and formatted *Advance Article* as soon as it is available.

You can find more information about *Accepted Manuscripts* in the **Information for Authors**.

Please note that technical editing may introduce minor changes to the text and/or graphics, which may alter content. The journal's standard **Terms & Conditions** and the **Ethical guidelines** still apply. In no event shall the Royal Society of Chemistry be held responsible for any errors or omissions in this *Accepted Manuscript* or any consequences arising from the use of any information it contains.

1   **The Role of Alkoxy Radicals in the Heterogeneous Reaction of Two Structural**
2   **Isomers of Dimethylsuccinic Acid**

3   Chiu Tung Cheng [a], Man Nin Chan [a,b*], Kevin R. Wilson [c*]

4   *[a] Earth System Science Programme, Faculty of Science, The Chinese University of Hong Kong,*
5   *Hong Kong, China*

6   *[b] The Institute of Environment, Energy and Sustainability, The Chinese University of Hong Kong,*
7   *Hong Kong, China*

8   *[c] Chemical Sciences Division, Lawrence Berkeley National Laboratory, Berkeley, CA, USA*

9   **Corresponding author: mnchan@cuhk.edu.hk; krwilson@lbl.gov*

10   **Abstract**

11   A key challenge in the understanding the transformation chemistry of organic aerosol is to quantify
12   how changes in molecular structure alter heterogeneous reaction mechanisms. Here we use two
13   model systems to investigate how the relative locations of branched methyl groups control the
14   heterogeneous reaction of OH with two isomers of dimethylsuccinic acid ($C_6H_{10}O_4$). 2,2-
15   dimethylsuccinic acid (2,2-DMSA) and 2,3-dimethylsuccinic acid (2,3-DMSA) differ only in the
16   location of the two branched methyl groups, thus enabling a closer inspection of how the
17   distribution of carbon reaction sites impacts the chemical evolution of the aerosol. The
18   heterogeneous reaction of OH with 2,3-DMSA (reactive OH uptake coefficient, $\gamma= 0.99\pm0.16$) is
19   found to be ~2 times faster than that of 2,2-DMSA ($\gamma= 0.41\pm0.07$), which is attributed to the larger
20   stability of tertiary alkyl radical produced by the initial OH abstraction reaction. While changes
21   in the average aerosol oxidation state (OS_C) and carbon number (N_C) with reaction for both isomers
22   are similar, significant differences are observed in the underlying molecular distribution of reaction
23   products. The reaction of OH with the 2,3-DMSA isomer produces two major reaction products:
24   a product containing a new alcohol functional group ($C_6H_{10}O_5$) formed by intermolecular
25   hydrogen abstraction and a C_5 compound formed via carbon-carbon (C-C) bond scission. Both of
26   these reaction products are explained by the formation and subsequent reaction of a tertiary alkoxy
27   radical. In contrast, the OH reaction with the 2,2-DMSA isomer forms four dominant reaction
28   products, the majority of which are C_5 scission products. The difference in the quantity of C-C
29   bond scission products for these two isomers is unexpected since decomposition is assumed to be
30   favored for the isomer with the most tertiary carbon sites (i.e. 2,3-DMSA). For both isomers, there
31   is a much larger abundance of C_6 alcohol relative to C_6 ketone products, which suggest that the
32   presence of the two branched methyl groups favors alkoxy formation from peroxy radical self-
33   reactions. These results reveal how isomeric structure ultimately controls the overall competition
34   between functionalization and fragmentation in these model systems.

35

36

1. Introduction

Organic aerosols contribute to a significant mass fraction of ambient aerosol carbon[1] and continuously undergo heterogeneous oxidation, by reactive collisions with gas-phase species such as OH, ozone (O_3) and nitrate radicals.[2] Atmospheric organic compounds have a wide range of properties such as polarity and volatility. Laboratory studies on the reactivity of organic aerosols toward OH radicals show that for chemically reduced (e.g., large alkanes) and oxygenated organic compounds (e.g., polyols and multifunctional acids), OH oxidation is fast and leads to a net increase in the degree of the oxygenation.[3-6] Functionalization reactions add polar functional groups (e.g., alcohol and carbonyl) to the parent molecule via peroxy radical reactions (i.e. Russell[7] and Bennett and Summers mechanisms[8]). The formation of smaller carbon number (N_C), volatile products are observed, where C-C bond scission (fragmentation) reactions occur via alkoxy radical intermediates (often termed "fragmentation"). While the average aerosol oxidation state (OS_C) always increases after oxidation, different extents of volatilization have been reported, depending on the yields and vapor pressures (or volatilities) of the fragmentation products. High molecular weight compounds or oligomers can also be formed, but the relative importance of the oligomerization for the overall chemical evolution of an aerosol remains unclear. At present, the relationship between molecular structure (e.g. carbon branching or number of oxygenated functional groups) and the competition between functionalization and fragmentation reactions remains poorly understood.

Gas-phase studies have clearly shown that molecular structure (e.g., linear, cyclic and branched hydrocarbons) plays a key role in the oxidation rate and mechanism of secondary organic aerosol formation. Gas-phase structure-activity relationships (SAR) suggest that hydrogen abstraction rate by OH radicals is faster at tertiary carbon sites than at primary or secondary carbon

60   atoms,[9] and thus the structure of a molecule plays a key role in determining the subsequent

61   oxidation kinetics and chemistry. Lim and Ziemann[10] showed that for the same carbon number,

62   reactions of branched alkanes (relative to linear and cyclic alkanes) with OH (with NO_x) have the

63   lowest aerosol yields. This is due to the propensity of branched molecules to form alkoxy radicals,

64   which can decompose to form smaller, more volatile products.[11]

65   To date, there are far fewer studies that have focused on how molecular structure influences

66   heterogeneous reaction pathways. Smith et al.[12] and Kessler et al.[4] found that carbon loss from an

67   aerosol increases as molecules in an aerosol become more highly oxidized. These observations

68   were explained in stochastic simulations by Wiegel et al.[13] that showed that for the

69   multigenerational oxidation of squalane, it is the population of activated alkoxy radicals that

70   controls fragmentation since their unimolecular decomposition rates can effectively compete with

71   other bimolecular reactions. Ruehl et al.[14] and Nah et al.[15] observed that the heterogeneous reaction

72   of OH with a branched alkane and alkene produced a larger number of smaller carbon number

73   products than their linear analogs. Zhang et al.[16] observed less mass loss of aerosols containing

74   molecules with cyclic moieties. Chan et al.[17] investigated the chemical transformation of succinic

75   acid aerosols during the heterogeneous OH oxidation. The aerosol mass spectral data revealed that

76   upon oxidation the average aerosol elemental composition evolved mainly through the formation

77   of C-C bond scission products with high OS_C and small N_C. Together these results all suggest that

78   fragmentation reactions become dominant pathways for aerosols containing oxygenated molecules,

79   which is in contrast to heterogeneous reactions of OH with chemically reduced molecules (i.e.

80   alkanes) that are dominated by functionalization at early oxidation stages.

81   Here we examine the molecular transformation of two structural isomers of

82   dimethylsuccinic acid (DMSA). The experiments are performed in an aerosol flow tube reactor. A

83   high resolution mass spectrometer coupled with an atmospheric pressure ionization source (Direct

84   Analysis in Real Time, DART)[18,19] is used to investigate the composition of DMSA aerosol in real

85   time. The structures of the two isomers, 2,2-dimethylsuccinic acid (2,2-DMSA) and 2,3-

86   dimethylsuccinic acid (2,3-DMSA), are shown in Table 1. The two isomers have the same

87   oxidation state (OS_C = -0.33) and carbon number (N_C = 6), but differ only in the locations of the

88   two branched methyl groups. 2,2-DMSA has one secondary and two primary carbon atoms, while

89   2,3-DMSA has two tertiary and two primary carbon sites. The difference in molecular distribution

90   of products observed during the heterogeneous reaction of these two structural isomers allows one

91   to assess the sensitivity of heterogeneous kinetics and chemistry to the location of branch points

92   in the molecule.

93   **2. Experiment**

94   **2.1 Aerosol flow tube reactor**

95   An aerosol flow tube reactor is used to investigate the OH initiated oxidation of two

96   structural isomers of aqueous DMSA droplets. A diagram of the setup is shown in Fig. 1. First,

97   aqueous droplets are generated by an atomizer (TSI Inc. Model 3076). A portion of the droplet

98   stream passes through a humidifier, maintained at a relative humidity (RH) of about 90% at 20°C.

99   The humidified droplet stream is then mixed with nitrogen, oxygen, hexane, and O_3, before

100 entering the aerosol flow tube reactor. The RH measured at the inlet of the reactor is about 85%.

101 A water jacket located outside the reactor is used to maintain the temperature inside the reactor at

102 20°C. Although the hygroscopicity of the two DMSA has not been measured, they are likely

103 aqueous droplets since the aerosol is always exposed to high RH. Before oxidation, the

104 composition of the aqueous DMSA droplets at RH=85% can be computed using an aerosol

105   thermodynamic model (Aerosol Inorganic-Organic Mixtures Functional groups Activity

106   Coefficients, AIOMFAC).[20] The initial concentration and density of 2,2-DMSA and 2,3-DMSA

107   are assumed to be the same. The droplets are predicted to have a mass fraction of solute of 0.69

108   and a molarity of 5.6M. The value of droplet density, ρ is estimated to be 1.175 g cm^{-3} using an

109   additivity rule and the known density and volume fraction of water and DMSA. The size

110   distribution of the aerosol leaving the reactor is measured using a scanning mobility particle sizer

111   (SMPS, TSI, 3936). Prior to oxidation, the mean surface weighted diameter for the aerosol is

112   145±1.76 nm for 2,2-DMSA and 150±0.95 nm for 2,3-DMSA (Table 1). Since the initial

113   composition and size of aqueous DMSA droplets are about the same for the two isomers, a direct

114   comparison between the data obtained from the two isomers is allowed to assess how the molecular

115   structure alters the heterogeneous oxidation processes.

116   The aerosol is oxidized by gas-phase OH radicals inside the reactor. OH radicals are

117   generated by the photolysis of O_3 at 254 nm in the presence of water vapor. The OH exposure (OH

118   radical concentration, *[OH]* × aerosol residence time, *t*) is varied by changing the O_3 concentration

119   and is quantified by measuring the decay of a gas-phase tracer (hexane).[12] The initial hexane

120   concentration, *[Hex]$_0$*, entering the reactor is about 100 ppb. The loss of hexane due to OH reaction

121   is determined by measuring the hexane concentration leaving the reactor, *[Hex]* using gas

122   chromatography (GC) coupled with a flame ionization detector. The hexane is pre-concentrated

123   for 3 min. in an absorbent trap prior to the GC analysis. With the known second order rate constant

124   *(k$_{Hex}$)* for the reaction of hexane with OH (k_{Hex} =5.2 ×10^{-12} cm^{3}molecule^{-1}s^{-1}), the OH exposure

125   can be determined,

126    $$\text{OH exposure} = -\frac{\ln([Hex]/[Hex]_0)}{k_{Hex}} = \int_0^t [OH]dt = \langle OH \rangle_t \cdot t \qquad \text{(Eqn. 1)}$$

127

128   where $\langle OH \rangle_t$ is the time averaged OH concentration. With a total flow rate of 2 L/min (an aerosol

129   residence time of 1.3 min), the reactor produces OH exposures ranging from 0 to 2.26×10^{12}

130   molecule cm^{-3} s. Upon exiting the reactor, the aerosol stream passes through an annular Carulite

131   catalyst denuder and an activated charcoal denuder that removes O_3 and other gas-phase species

132   from the aerosol stream, respectively. A portion of the aerosol stream is then sampled by the SMPS

133   for size measurements. The remaining flow is directed into an ionization region of the mass

134   spectrometer, which is an open space between a DART ionization source and an atmospheric inlet

135   of a mass spectrometer (MS, ThermoFisher, Q Exactive Orbitrap), for real time chemical

136   characterization.

137   **2.2 Atmospheric Pressure Aerosol Mass Spectrometer**

138   The DART ionization source (IonSense: DART SVP) is interfaced to a mass spectrometer

139   and operated in negative ionization mode with helium as the ionizing gas. The desorption angle

140   (the angle of the DART ionization source relative to the MS inlet) and desorption distance (the

141   distance between the orifice of the DART ionization source and the MS inlet) are set to be 45° and

142   1.5 cm, respectively. The heater inside the DART source is set to 500°C. Before entering the

143   ionization region, the aerosol stream passes through an external heater (150°C) to fully vaporize

144   the aerosol in order to obtain bulk chemical composition. The DMSA and its reaction products are

145   ionized by the reactive species in the DART ionization source. The resulting ions are then sampled

146   by the mass spectrometer. Mass spectra are collected at 1 s intervals over a scan range from *m/z*

147   70 – 700. Each mass spectrum is averaged over a 5 min sampling time with a mass resolution of

148   about 140,000. The mass calibration is performed with standard solutions before experiments. The

149   mass spectra are analyzed using the Xcalibar software (Xcalibar Software, Inc., Herndon, VA,

150   USA).

151   As described by Cody et al.[18] and Cody [19], in the negative ionization mode, the electrons

152   produced through Penning ionization in the DART ionization source are captured by atmospheric

153   O_2 in the ionization region to produce anionic oxygen (O_2^-). The O_2^- reacts with gas phase species

154   (M) through proton abstraction to yield deprotonated molecular ions, $[M-H]^-$. The mass spectra

155   of carboxylic acids, dicarboxylic acids, and multifunctional organic acids are dominated by their

156   corresponding $[M-H]^-$, which are resulted from the proton abstraction from the carboxylic acid

157   group.[21, 22] As discussed below, nearly all of the reaction products likely contain one or two

158   carboxylic acid functional group(s), which would be detected as $[M-H]^-$.

159   **3. Results and Discussions**

160   The following sections are organized as follows: First, the heterogeneous kinetics and OH

161   uptake coefficients of the two DMSA isomers are presented (Section 3.1). Second, the average

162   aerosol elemental composition is evaluated based on the abundance and chemical formula of the

163   observed reaction products (Section 3.2). Third, a reaction mechanism is proposed to explain the

164   formation of the major products (Section 3.3 and 3.4). Based on the molecular distribution of

165   reaction products, we analyze how isomer structure influences: (1) the preferred H abstraction site

166   (backbone carbon site vs. branched methyl group) by OH radicals (Section 3.5), (2) the importance

167   of alkoxy radical chemistry (Section 3.6), and (3) the overall competition between the

168   functionalization and fragmentation (Section 3.7).

169   **3.1 Heterogeneous oxidation kinetics: Uptake coefficients**

170   Fig. 2 shows the mass spectra of 2,2-DMSA and 2,3-DMSA before and after reaction with

171   OH (in the presence of O_2). For the 2,2-DMSA, in addition to the unreacted parent DMSA (m/z =

172   145), which contributes about half of the total ion signal, 4 major products are observed after

173   oxidation: $C_6H_{10}O_5$ (*m/z* = 161), $C_5H_8O_3$ (*m/z* = 115), $C_5H_8O_4$ (*m/z* = 131), and $C_5H_8O_5$ (*m/z* =

174   147). For the 2,3-DMSA, only two new major peaks are observed in the mass spectrum: $C_6H_{10}O_5$

175   (*m/z* = 161) and $C_5H_8O_3$ (*m/z* = 115). While at this OH exposure, the unreacted 2,3-DMSA is the

176   largest peak, there are a number of additional smaller peaks each with a relative abundance less

177   than 1%. The molecular formula of the major products is listed in Table 2.

178   To quantify the heterogeneous kinetics, the decay of 2,2-DMSA and 2,3-DMSA are plotted

179   as a function of OH exposure (Fig. 3). The significant loss of the two isomers can be explained

180   rapid diffusion of reaction products from the bulk to the surface on the timescale of the reaction.

181   From an exponential fit of the data, the OH rate constant, *k*, for 2,2-DMSA and 2,3-DMSA is

182     $5.32\pm0.35 \times 10^{-13}$ cm^3 molecule^{-1} s^{-1} and $1.23\pm0.08 \times 10^{-12}$ cm^3 molecule^{-1} s^{-1}, respectively can be

183   obtained. From *k*, the reactive OH uptake coefficient γ, defined as the fraction of reactive OH

184   collisions with DMSA is:[12]

$$\gamma = \frac{4kD_p\rho N_A}{6\bar{c}M_w}$$ (Eqn. 2)

186   where D_p is the mean surface weighted aerosol diameter, ρ is the aerosol density, N_A is Avogadro's

187   number, $\bar{c}$ is the average speed of OH radicals, and M_w is the molecular weight of the parent

188   molecule. From eqn. 2, γ for 2,2-DMSA and 2,3-DMSA are computed to be 0.41±0.07 and

189   0.99±0.16, respectively. This indicates that the reactivity of 2,3-DMSA towards OH radicals is

190   about 2 times faster than that of 2,2-DMSA. Since some uncertainties in the parameters cancel out

191   when a ratio is used, the relative reactivity of the two isomers is a more robust metric than the

192   absolute value when comparing the oxidative kinetics and uptake coefficients of the two isomers.

193   The difference in OH reactivity is likely due to the enhanced stability of the carbon-centered

194   radical formed after the hydrogen abstraction, since an alkyl radical formed by hydrogen

195   abstraction at a tertiary carbon site is more stable than at a secondary or primary carbon site. γ

196   values larger than 1 have been reported for the heterogeneous oxidation of organic aerosol,[17] which

197   can be attributed to the secondary chemistry occurred in the aerosol-phase. While in this study the

198   calculated γ for the two DMSA isomers are less than 1, the secondary chemistry due to alkoxy

199   abstraction reactions are likely the major reaction pathways and will be discussed in Section 3.6.

200   The relative reactivity of the aqueous DMSA droplets towards OH radicals can be

201   compared to a structure activity relationship (SAR) model proposed for dilute aqueous solution.[23]

202   The OH rate constant of 2,3-DMSA is estimated to have a value close to that of 2,2-DMSA (k_{OH+}

203   $_{2,2-DMSA}$: $k_{OH+2,3-DMSA} = 1.02:1$). Since the initial size of the aerosol for the two DMSA isomers are

204   very similar (Table 1), $\gamma_{OH+2,2-DMSA}$ and $\gamma_{OH+2,3-DMSA}$ are estimated to be about the same using eqn.

205   1. On the other hand, the measured γ reveals that the more concentrated aqueous DMSA droplets

206   (5.6M) exhibits a positional selectivity for hydrogen abstraction by OH radicals ($\gamma_{OH+2,2-DMSA}$:

207   $\gamma_{OH+2,3-DMSA} = 1:2.3$). The difference in uptake coefficients observed here is more consistent with

208   the predictions using a SAR model proposed for gas-phase chemistry.[9] This may be explained

209   either by reaction of OH at a surface (rather than in bulk) or by differences between the highly

210   concentrated aqueous DMSA droplets and the SAR models that are formulated for dilute aqueous

211   solutions.

212   **3.2 Average aerosol elemental composition**

213   For the two DMSA isomers, the ion signals corresponding to reaction products increase

214   with increasing OH exposure (Fig. S1 and S2, supporting material). Based on the exact mass and

215   relative abundance of the reaction product ions, the average aerosol elemental composition (O/C

216   and H/C ratios) can be estimated at a given OH exposure as follows.[17]

217 $$O/C = \sum_i (O/C)_i I_i \qquad \text{(Eqn. 3)}$$

218 $$H/C = \sum_i (H/C)_i I_i \qquad \text{(Eqn. 4)}$$

219   where $(O/C)_i$, $(H/C)_i$, and I_i are the O/C, H/C, and relative ion signal of reaction product i

220   respectively. Here we assume that the ionization efficiencies for all the products are the same and

221   the reaction products in the mass spectra account for all products formed in the aerosol after

222   oxidation. Before the oxidation, the total ion signal normalized by the aerosol mass of 2,2-DMSA

223   and 2,3-DMSA are 1.83×10^6 and 1.68×10^6 /(μg m^{-3}), respectively. These results suggest that

224   the ionization efficiencies of the two parent DMSA isomers are nearly the same. To our knowledge,

225   authentic standards are not available for many oxidation products. Therefore, we here assume that

226   the ionization efficiencies of the two DMSA isomers and the observed products are the same. We

227   also acknowledge that certain products (e.g., organic peroxides and oligomers) may not be detected

228   efficiently in the mass spectra generated by the DART. Although as will discussed below, the most

229   abundant first generation products can be well explained by the established mechanisms.

230   A van Krevelen diagram, H/C ratio vs. O/C ratio, is used to investigate the change in

231   average aerosol elemental composition as a function of oxidation lifetime (Fig. 4a and 4b). The

232   oxidation lifetime is defined as the OH exposure multiplied by the OH rate constant. Before

233   oxidation, 2,2-DMSA and 2,3-DMSA have the same elemental composition (O/C = 0.67 and H/C

234   = 1.67). As the oxidation lifetime increases, the O/C ratio increases while the H/C ratio decreases.

235   The slopes from a linear fit to the data are very similar for 2,2-DMSA (-0.61±0.02) and 2,3-DMSA

236   (-0.72±0.06). At the maximum oxidation lifetime (or maximum OH exposure), the two DMSA

237   isomers exhibit different extents of oxidation. 2,3-DMSA undergoes a larger change in O/C and

238   H/C ratios (ΔO/C = 0.088±0.003, ΔH/C = -0.065±0.014) than that of 2,2-DMSA (ΔO/C =

239   0.062±0.003, ΔH/C = -0.038±0.018). However, it is noted that when comparing the H/C and O/C

240   ratios changes at the same oxidation lifetime (about one), the extent of the oxidation for the 2,2-

241   DMSA (ΔO/C = 0.062±0.003, ΔH/C = -0.038±0.018) is slightly larger than 2,3-DMSA (ΔO/C =

242   0.04±0.004, ΔH/C = -0.017±0.022).

243   As shown in Fig. 4c and 4d (OS_C vs. N_C space), at the same oxidation lifetime, 2,2-DMSA

244   exhibits a larger increase in OS_C (ΔOS_C= 0.162±0.001) and a larger decrease in the N_C (ΔN_C= -

245   0.390±0.0226) compared to 2,3-DMSA (ΔOS_C= 0.097±0.001, ΔN_C= -0.150±0.289). This indicates

246   that fragmentation processes are more significant in the reaction of 2,2-DMSA, leading to the

247   formation of smaller, more oxygenated fragmentation products. Although there are small

248   differences in the extent of oxygenation and overall changes in average aerosol elemental

249   composition of both DMSA isomers upon reaction with OH, the molecular distributions of the

250   products of these two isomers differ significantly. In following sections, reaction schemes are

251   proposed to explain the formation of the observed products and to better understand how the

252   evolution of the average aerosol elemental composition depends on the underlying distribution of

253   reaction products.

254   **3.3 Reaction Mechanisms**

255   The reaction mechanisms that lead to the formation of the observed products are proposed

256   based on the exact mass measurements reported here and previously reported condensed-phase

257   reaction pathways.[2, 24, 25] The proposed reaction schemes follow closely the generalized OH radical

258   initialized oxidation mechanism shown in Fig. 5. The reaction is initiated when an OH radical

259   abstracts a hydrogen atom on a parent molecule to form an alkyl radical. An O_2 molecule quickly

260   reacts with the alkyl radical to form a peroxy radical. The reaction between two peroxy radicals

11

261   forms a tetroxide intermediate, which subsequently undergoes functionalization reactions such as

262   Bennett and Summers reaction (**R1**)[8] and Russell mechanism (**R2**)[7]. These reactions both increase

263   the molecular weight and polarity of the parent molecule by the addition of a new carbonyl or

264   alcohol functional group (functionalization) to the carbon skeleton. Alternatively, the tetroxide

265   intermediate can decompose, producing O_2 and two alkoxy radicals. This alkoxy intermediate can

266   react through hydrogen abstraction (**R3**), with O_2 (**R4**), or undergo β-scission (**R5**). Pathways (**R3**)

267   and (**R4**) yield functionalization products without C-C bond scission (i.e. functionalization). The

268   β-scission channel (**R5**) is the most important general pathway to produce smaller molecular

269   weight products (i.e. fragmentation). In principle, oligomerization could occur, but is not

270   considered here since high molecular weight products with N_C larger than 6 are not detected in the

271   mass spectra. Nevertheless, it is possible that some oligomers may thermally decompose during

272   the DART analysis.[17] Based on the exact mass measurements of the products formed in the OH +

273   DMSA reaction, the relative importance of these generalized pathways shown in Fig. 5 are

274   evaluated below.

3.4 Heterogeneous OH oxidation of two DMSA isomers

276   As illustrated in Fig. 2, for both isomers, there are only a few products peaks in the

277   spectrum and as such the following discussion of reaction schemes will be primarily focused on

278   the mostly likely formation pathways of these products, which are shown in Table 2. The kinetic

279   evolutions of these major products (Fig. S1 and S2) are consistent with first-generation products.

3.4.1 Reaction of OH with 2,3-DMSA

281   For the 2,3-DMSA (Fig. 2), two new major peaks are observed in the mass spectrum: one

282   C_6 functionalization product ($C_6H_{10}O_5$) and one C_5 fragmentation product ($C_5H_8O_3$). Scheme 1

283   shows that the OH oxidation of 2,3-DMSA can be initiated by abstraction of a hydrogen atom

284   located either on the backbone carbon site (Path A) or on the branched methyl group (Path B) to

285   yield two distinct peroxy radicals. When the hydrogen atom abstraction occurs at one of the two

286   tertiary backbone carbons (Path A), a tertiary peroxy radical is formed. The only stable

287   functionalization product that is possible at this tertiary carbon site is the hydroxy-DMSA

288   ($C_6H_{10}O_5$). The most likely formation pathway for this major C_6 functionalization product is

289   through the formation of a tertiary alkoxy radical, which can subsequently abstract an H atom from

290   a neighboring molecule as shown by **R3** in Scheme 1. It could also be possible, although unlikely,

291   that once formed the tertiary peroxy radical could react with a primary peroxy radical (formed via

292   Path B, Scheme 1) to form the hydroxy-DMSA ($C_6H_{10}O_5$). However, the co-product of this tertiary

293   peroxy + primary peroxy radical reaction would be by necessity a carbonyl ($C_6H_8O_5$) located on

294   the branched methyl group. However, as shown in Fig. S1, the signal in the mass spectrum

295   corresponding to this carbonyl product is ~32-50 times smaller than the hydroxy-DMSA

296   ($C_6H_{10}O_5$). As such, the most likely formation pathway for the hydroxy-DMSA ($C_6H_{10}O_5$) appears

297   to be via an alkoxy H abstraction channel (**R3**). Furthermore, decomposition of the alkoxy

298   intermediate would naturally form the major C_5 product ($C_5H_8O_3$) or a more volatile C_3

299   fragmentation product that is only detected in small abundance presumably due to its higher

300   volatility.

301   The initial OH reaction could also occur on the branched methyl groups (Path B). The

302   reactions of two peroxy radicals at the primary carbon site could form a structural isomer of the

303   hydroxy-DMSA ($C_6H_{10}O_5$) product and a keto-DMSA ($C_6H_8O_5$). The alkoxy radicals resulting

304   from the peroxy self-reactions can undergo hydrogen abstraction (**R3**) or O_2 abstraction (**R4)** to

305   form these two C_6 functionalization products. However, as described above, the keto-DMSA

306   ($C_6H_8O_5$) is detected only in very small abundance and therefore it seems highly unlikely that the

307   large signal from the hydroxy-DMSA ($C_6H_{10}O_5$) originates from this path. Overall, the two major

308   products of the reaction of OH with 2,3-DMSA can both be attributed to a common tertiary alkoxy

309   radical intermediate formed via self-reaction of two tertiary peroxy radicals (Scheme 1, Path A).

310   **3.4.2 Oxidation of 2,2-DMSA**

311   As shown in Fig. 2, the OH reaction with the 2,2-DMSA isomer forms four major products:

312   one C_6 functionalization product ($C_6H_{10}O_5$) and three C_5 fragmentation products ($C_5H_8O_3$, $C_5H_8O_4$,

313   and $C_5H_8O_5$). Scheme 2 shows that when the hydrogen abstraction occurs either on the backbone

314   carbon site (Path A) or the branched methyl group (Path B), two isomers of hydroxy-DMSA

315   ($C_6H_{10}O_5$) and of keto-DMSA ($C_6H_8O_5$) can be formed by the reaction of two peroxy radicals (**R1**

316   and **R2**). While the peroxy self-reactions produce two alkoxy radicals, they can abstract a hydrogen

317   atom from a neighboring molecule (**R3**) to form the hydroxy-DMSA ($C_6H_{10}O_5$) or react with an

318   O_2 molecule **(R4)** to form the keto-DMSA ($C_6H_8O_5$) without fragmentation. However, similar to

319   the OH reaction with 2,3-DMSA, the keto-DMSA ($C_6H_8O_5$) is not observed. Therefore it is highly

320   likely that the hydroxy-DMSA ($C_6H_{10}O_5$) is formed by intermolecular hydrogen abstraction (**R3**)

321   by alkoxy radicals formed at the two different carbon sites.

322   The formation of major C_5 fragmentation products is mainly attributed to the β-scission of

323   the alkoxy radical. When the hydrogen abstraction is initiated at the backbone carbon site (Path

324   A), a major C_5 carboxylic acid ($C_5H_8O_3$) is produced from the decomposition of the alkoxy radical,

325   after which the aldehydic hydrogen atom can be rapidly oxidized to form a carboxylic acid

326   functional group. This could be one potential route for the formation of the other major C_5

327   fragmentation product (C_5 dicarboxylic acid, $C_5H_8O_4$).

328   When the hydrogen atom is abstracted from the branched methyl group (Path B), the

329   decomposition of the alkoxy radical can easily eliminate formaldehyde (CH_2O). This process

330   might seem unusual, but the elimination of formaldehyde forms a stable tertiary C_5 alkyl radical

331   making this pathway more favorable. Once formed, the tertiary C_5 alkyl radical reacts quickly with

332   an O_2 molecule to form a tertiary C_5 peroxy radical, which then reacts with another peroxy species

333   to form a tertiary alkoxy radical. This is consistent with the very small abundance of carbonyl

334   products, which are co-products formed via the Russell mechanism (**R2**). The C_5 alkoxy radical

335   can abstract an H atom from a neighboring molecule (**R3**) thus explaining the major C_5

336   dicarboxylic acid ($C_5H_8O_5$) observed in the mass spectrum.

337   For both DMSA isomers, the unreacted parent DMSA and reaction products shown in

338   schemes 1 and 2 represent 96.8 and 94.2% of the total ion signals for 2,3-DMSA and 2,2-DMSA,

339   respectively at oxidation lifetime of about 1. When the oxidation proceeds further, the first-

340   generation products can be oxidized by OH radicals. Since second- or higher-generation products

341   do not contribute significantly to the total ion signals and the abundance of these individual

342   products is typically less than 2% of total signal (Fig. S1 and S2), their formation mechanisms are

343   not presented here. While the formation of the major observed products in the oxidation of the two

344   DMSA isomers can be well explained by the general reaction schemes (Fig. 5), the molecular

345   distribution of the reaction products provides new insights into OH reaction sites and the overall

346   importance of alkoxy radical chemistry on product formation.

347   **3.5 OH reaction site: Carbon backbone vs. branched methyl group**

348   The exact location of the carbon site where the H atom is abstracted by OH radicals governs

349   the subsequent product formation chemistry. Thus, the molecular distribution of the observed

350   products can be, in principle, used to examine where the initial hydrogen abstraction occurs. For

351   both 2,3-DMSA (section 3.4.1) and 2,2-DMSA (section 3.4.2), the structural isomers of the

352   functionalization products cannot be differentiated from the exact mass measurements alone. In

353   contrast, the fragmentation products formed from hydrogen abstraction at the two different carbon

354   locations can be distinguished by their chemical formula based on the proposed reaction pathways.

355   Fragmentation products with distinct chemical formula (as shown in Schemes 1 and 2) can be

356   grouped based on their OH reaction sites (backbone carbon site vs. branched methyl group). This

357   goal of simple analysis is to qualitatively assess, which carbon site is more favorably for hydrogen

358   abstraction during the OH oxidation of parent DMSA.

359   Fig. 6a and 6b show the relative abundance of the fragmentation products grouped by OH

360   reaction site (backbone vs. branched methyl group) as a function of oxidation lifetime. For both

361   2,2-DMSA and 2,3-DMSA, the fragmentation products formed via hydrogen abstraction at the

362   backbone carbon site are clearly more abundant than those products formed via reaction on the

363   branched methyl group. This can be explained by the enhanced stability of the alkyl radical formed

364   at a secondary or tertiary carbon site (backbone carbon site) relative to a primary carbon (branched

365   methyl group). Although the branching ratios for specific reaction pathways cannot be directly

366   assigned, the results of this simple analysis are consistent with predictions from gas-phase SAR,[9]

367   which predict that the ratio of H abstraction rates at the backbone carbon site vs. branched methyl

368   group to be 2.6 and 10.6 for 2,2-DMSA and 2,3-DMSA, respectively. The ratio also suggests a

369   smaller overall difference in the OH reactivity of hydrogens at secondary and primary sites, in

370   contrast to the much larger difference between abstraction rates at tertiary vs. primary sites. This

371   is consistent to the observation that the ratio of fragmentation products formed at different carbon

372   sites is isomer dependent. Thus, not unexpectedly, hydrogen abstraction on the branched methyl

373   group is a more significant pathway for 2,2-DMSA than 2,3-DMSA.

374   It is noted that for a primary reaction, the ratios of fragmentation products formed at

375   different carbon sites would be expected to be independent of oxidation lifetimes. For the two

376   isomers, secondary chemistry (e.g. hydrogen abstraction by alkoxy radicals) could play a role in

377   the formation of reaction products. The relative importance of the secondary chemistry to primary

378   reactions may change with the oxidation lifetimes (or OH exposures), which would affect the

379   chemical evolution of the reaction products and the final aerosol composition. This might explain

380   why the ratio depends upon oxidation lifetimes.

381   **3.6 Importance of alkoxy radical chemistry: Large hydroxy-DMSA vs. keto-DMSA ratio**

382   For both isomers, there is clearly a larger abundance of C_6 alcohol products relative to C_6

383   ketone products (i.e. large hydroxy-DMSA vs. keto-DMSA) (Table 2). These observations cannot

384   be simply explained by well-known condensed-phase functionalization reactions such as the

385   Bennett and Summers (**R1**) and Russell (**R2**) mechanisms since the expected ratio of hydroxy-

386   DMSA to keto-DMSA would be either 1 (Russell mechanism only) or 0 (Bennett and Summers

387   reaction only). One explanation for the observed large alcohol-to-ketone ratios is the presence of

388   the two bulky branched methyl groups (adjacent to the carboxylic acid groups). These methyl

389   groups may sterically hinder the appropriate arrangement of the two peroxy radicals into a cyclic

390   tetroxide intermediate proposed in the Russell and Bennett and Summers mechanisms necessary

391   for the formation of stable ketone and alcohol products. Rather this steric effect may, in turn, favor

392   the formation of alkoxy radicals (and O_2 as a coproduct). Once formed, as shown in Fig. 5, the

393   alkoxy radical can form the hydroxy-DMSA (**R3**) via H abstraction.   The low abundance or

394   absence of the keto-DMSA product would also indicate that the reaction with O_2 (**R4**) is less

395   favorable. Thus the major products observed here can be best explained by the intermolecular

396   hydrogen abstraction (**R3**) and C-C bond scission of alkoxy radicals (**R5**).

397   These results are in large contrast to our earlier study of succinic acid,[17] where we found

398   that at oxidation lifetime of about 1, the ratio of hydroxy-succinic acid and keto-succinic acid is

399   near 1, suggesting Bennett and Summers reaction (**R1**) and Russell mechanism (**R2**) are important

400   reaction pathways when the methyl groups are absent. These results also show that DART

401   ionization can effectively detect ketone products if they are formed as well as support the

402   hypothesis that for the two DMSA isomers, it is the addition of two branched methyl groups to the

403   backbone of the succinic acid that enhances the formation of alkoxy radicals from the peroxy

404   radical self-reactions.

405   **3.7 Importance of alkoxy radical chemistry: Fragmentation vs. functionalization**

406   As discussed above, alkoxy radical chemistry appears to play a dominant role in the

407   formation of the observed products for the two DMSA isomers. Once formed, the alkoxy radical

408   can either abstract a hydrogen atom from a neighboring molecule without fragmentation (**R3**) or

409   decompose to yield smaller products (**R5**). The relative abundance of fragmentation vs.

410   functionalization products may provide insights on how the position of the branched methyl groups

411   determines the fate of the alkoxy radical. As shown in Fig. 6c, the abundance of fragmentation

412   products ($N_C < 6$) is greater than that of functionalization products ($N_C = 6$) for 2,2-DMSA. This

413   is in contrast to 2,3 DMSA where functionalization products are more abundant than fragmentation

414   (Fig. 6d). These results are somewhat unexpected since fragmentation might be expected to be

415   more favorable for 2,3-DMSA since self -reactions of two tertiary peroxy reactions can only

416   produce alkoxy radicals.

417   Recent studies suggest that the presence of functional groups on adjacent carbon atoms can

418   alter the decomposition of alkoxy radical in the gas-phase chemistry[26, 27, 28]. An alcohol or carbonyl

419   functional group located on the α- and β-carbon can lower the activation energy required for the

420   decomposition of alkoxy radical and can thus enhance the fragmentation process. A SAR model

421   for substituted-alkoxy decomposition has been developed considering the nature and number of

422   alkyl-, carbonyl-, hydroxyl and/or other functional groups on the α- and β-carbon. [27, 28] For the

423   DMSA isomers, nearly equally low barriers (about 2 to 2.5 kcal/mol) are predicted for the

424   decomposition of the two alkoxy radicals formed on the carbon backbone for the two isomers. It

425   is because the carbonyl- and hydroxyl functional group on that β-carbon (carbon-center of the

426   leaving radical) significantly lower the decomposition barrier, whereas the alkyl groups on α-

427   carbon (carbon of the forming carbonyl group) only have a marginal effect. The model predicts a

428   slightly faster decomposition rate for the tertiary alkoxy radical from 2,3-DMSA since there are

429   one more alkyl group on the α-carbon,. The effect to the barrier by the methyl groups on other

430   positions is marginal. Overall, these results suggest that the decomposition would not be

431   significantly affected by the presence of branched methyl groups for the two isomers. One

432   possibility is that the relative stability of the alkoxy radical that is formed, which may enhance the

433   hydrogen abstraction rates from neighboring molecules in the condensed-phase. Hence, it appears

434   that alkoxy radicals formed at the tertiary carbon sites in 2,3-DMSA are more likely to abstract a

435   hydrogen atom from a neighboring molecule than decompose compared to 2,2-DMSA. However,

436   more work is needed to verify this hypothesis.

437   The functionalization and fragmentation products are mainly formed via common alkoxy

438   radical chemistry. As shown in Fig. 6c and 6d, both products evolve at a comparable rate upon

439   oxidation. This would suggest that the overall rate of unimolecular decomposition of the alkoxy

440   radical is competitive with intermolecular hydrogen abstraction. For the two isomers, the

441   unimolecular decomposition rates of the alkoxy radical predicted by the SAR model are in order

442   of $10^{11}\,\text{s}^{-1}$ at 298 K. Assuming the [RH] is approximately equal to the initial concentration of parent

443   DMSA molecules ($\sim 10^{21}$ molecule cm^{-3}), the estimated second order rate constant for the

444   intermolecular hydrogen abstraction (RO· + RH) would have to be of order $\sim 10^{-10}$ cm^{3}molecule^{-}

445   ^{1}s^{-1}. These estimated values are larger than the diffusion limit in the condensed phase and previous

446   literature reports for the second order rate constant for the RO· + RH reaction, which ranges from

447   10^{-13} to 10^{-15} cm^3 molecule^{-1}s^{-1}.[29] One possible explanation is that the SAR model does not take

448   into account the hydrogen bonding between the two terminal carboxyl functional groups. This

449   strong hydrogen bonding might lower the SAR predicted decomposition rates, making the

450   hydrogen abstraction by the alkoxy radicals more competitive. This may also attribute to

451   differences between the chemistry in highly concentrated aqueous DMSA droplets and the SAR

452   models that are formulated for either gas-phase reactions or very dilute solutions.

453   **4. Summary**

454   Based on the exact mass measurements and proposed reaction pathways, the position of

455   the branched methyl groups is observed to play a key role in determining the heterogeneous OH

456   oxidation of two structural isomers, 2,2-DMSA and 2,3-DMSA. Kinetic measurements show that

457   the OH decay of 2,3-DMSA is faster than that of 2,2-DMSA by about a factor of 2. This can be

458   explained by the larger stability of a tertiary alkyl radical formed by the initial hydrogen abstraction.

459   A large alcohol-to-ketone ratio is observed for the functionalization products of both isomers. This

460   is explained by the preference to form alkoxy radicals from peroxy self-reactions, which

461   subsequently undergo intermolecular hydrogen abstraction or decomposition. The overall

462   oxidation is likely dominated by the alkoxy radical chemistry for the highly branched DMSA,

463   which is in large contrast to succinic acid, its less branched counterpart.

464   At the same oxidation lifetime, the contribution of fragmentation products to the total

465   reaction products is larger for 2,2-DMSA than 2,3-DMSA, suggesting, somewhat unexpectedly,

466   that fragmentation is not simply related to the prevalence of tertiary peroxy radicals. This suggests

467   that the branching ratios between fragmentation and functionalization depend upon other factors.

468   The hydrogen abstraction rate of alkoxy radicals might be related to its overall stability and may

469   be a more significant effect in the particle-phase than in the gas-phase. Overall, the molecular

470   structure of the two DMSA isomers is useful to understand the oxidation kinetics, preferential OH

471   reaction sites, and overall competition between fragmentation and functionalization processes

472   during the early oxidation stages.

473   **5. Acknowledgements**

479

480

Notes and References

481

482 1. M. Hallquist, J. Wenger, U. Baltensperger, Y. Rudich, D. Simpson, M. Claeys, J. Dommen, N.

483   Donahue, C. George and A. Goldstein, *Atmos. Chem. Phys.*, 2009, **9**, 5155–5236.

484 2. I. J. George and J. P. D. Abbatt, *Nature Chem.*, 2010, **2**, 713–722.

485 3. J. H. Kroll, J. D. Smith, D. L. Che, S. H. Kessler, D. R. Worsnop and K. R. Wilson, *Phys.*

486   *Chem. Chem. Phys.,* 2009, **11**, 8005–8014.

487 4. S. H. Kessler, J. D. Smith, D. L. Che, D. R. Worsnop, K. R. Wilson and J. H. Kroll, *Environ.*

488   *Sci. Technol.*, 2010, **44**, 7005–7010.

489 5. S. H. Kessler, T. Nah, K. E. Daumit, J. D. Smith, S. R. Leone, C. E. Kolb, D. R. Worsnop, K.

490   R. Wilson and J. H. Kroll, *J. Phys. Chem. A*, 2012, **116**, 6358–6365.

491 6. J. H. Slade and D. A. Knopf, *Phys. Chem. Chem. Phys.*, 2013, **15**, 5898–5915.

492 7. G.A. Russell, *J. Am. Chem. Soc.*, 1957, **79**, 3871-3877.

493 8. J.E. Bennett and R. Summers, *Can. J. Chem.*, 1974, **52**, 1377-1379

494 9. E. S. Kwok and R. Atkinson, *Atmos. Environ.*, 1995, **29**, 1685–1695.

495 10. Y. B. Lim and P. J. Ziemann, *Environ. Sci. Technol.*, 2009, **43**, 2328–2334.

496 11. J. L. Jimenez et al., *Science*, 2009, **326**, 1525–1529.

497 12. J. D. Smith, J. H. Kroll, C. D. Cappa, D. L. Che, C. L. Liu, M. Ahmed, S. R. Leone, D. R.

498   Worsnop and K. R. Wilson, *Atmos. Chem. Phys.,* **2009**, 9, 3209–3222.

499 13. A. A. Wiegel, K. R. Wilson, W. D. Hinsberg and F. A. Houle, *Phys. Chem. Chem. Phys.,* 2015,

500   **17**, 4398-4411.

501 14. C. R. Ruehl, T. Nah, G. Isaacman, D. R. Worton, A.W.H. Chan, K. R. Kolesar, C. D. Cappa,

502   A.H. Goldstein and K.R. Wilson, *J. Phys. Chem. A,* 2013, **117**, 3990–4000.

503   15. T. Nah, H. Zhang, D. R. Worton, C.R. Ruehl, B. B. Kirk, A. H. Goldstein, S. R. Leone and

504   K.R. Wilson, *J. Phys. Chem. A*, 2014, **118**, 11555–11571.

505   16. H. Zhang, C. R. Ruehl, A. W. H. Chan, T. Nah, D. R. Worton, G. Isaacman, A. H. Goldstein

506   and K. R. Wilson, *J. Phys. Chem. A*, 2013, **117**, 12449–12458.

507   17. M. N. Chan, H. Zhang, A.H. Goldstein and K.R. Wilson, *J. Phys. Chem. C*, 2014, **118**, 28978-

508   28992.

509   18. R. B. Cody, J. A. Laramee and H. D. Durst, *Anal. Chem.*, 2005, **77**, 2297–2302.

510   19. R. B. Cody, *Anal. Chem.*, 2008, **81**, 1101–1107.

511   20. A. Zuend, C. Marcolli, B. P. Luo and T. Peter, *Atmos. Chem. Phys.*, 2008, **8**, 4559–4593.

512   21. M. N. Chan, T. Nah and K. R. Wilson, *Analyst*, 2013, **138**, 3749–3757.

513   22. T. Nah, M. N. Chan, S. R. Leone and K. R. Wilson, *Anal. Chem.,* 2013, **85**, 2087–2095.A.

514   Monod, L. Poulain, S. Grubert, D. Voisin and H. Wortham, *Atmos Environ.*, 2005, **39**, 7667–

515   7688.

516   23. N. K. V. Leitner and M. Dore, *J. Photochem. Photobio. A,* 1996, **99**, 137–143.

517   24. L. Yang, M. B. Ray, E. Y. Liya , *Atmos. Environ.*, 2008, **42**, 868–880.R. Atkinson, *Atmos.*

518   *Environ.*, 2007, **41**, 8468–8485.

519   25. J. Peeters, G. Fantechi and L. Vereecken, *J. Atmos. Chem.* 2004, **48**, 59-80.

520   26. L. Vereecken and J. Peeters, *Phys. Chem. Chem. Phys.*, 2009, **11**, 9062-9074.

521   27. E. T. Denisov and I. B. Afanas' ev, *Oxidation and antioxidants in organic chemistry and*

522   *biology*, CRC press, 2005.

523

524 Table 1 Properties, rate constants, and reactive OH uptake coefficients of 2,2-dimethylsuccinic
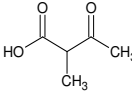525 acid (2,2-DMSA), and 2,3-dimethylsuccinic acid (2,3-DMSA).

526
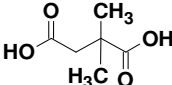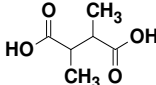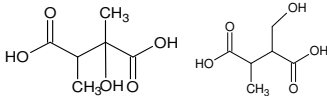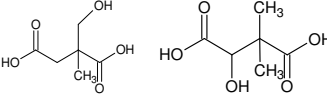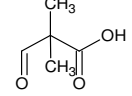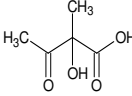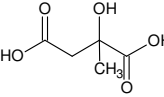
	2,2-DMSA	2,3-DMSA
Chemical structure		
Chemical formula	$C_6H_{10}O_4$	
Oxygen-to-carbon ratio, O/C	0.67	
Hydrogen-to-carbon ratio, H/C	1.67	
Carbon oxidation state, OS_C	-0.33	
Carbon number, N_C	6	
Number of carbon		
Primary	2	2
Secondary	1	0
Tertiary	0	2
Results from this work		
(aqueous droplet) OH rate constant, k ($\times 10^{-13}$ cm^3 molecule^{-1} s^{-1})	5.32 ± 0.35	12.3 ± 0.8
Reactive OH uptake coefficient, γ	0.41 ± 0.07	0.99 ± 0.16
Initial aerosol diameter (nm)	145 ± 1.76	150±0.95

527 Table 2 The major observed products of 2,2-DMSA and 2,3-DMSA. The relative abundance of
528 the products at about 1 oxidation lifetime is reported.

Chemical formula	Proposed chemical structure	Molecular weight	Oxidation state	Relative abundance (%)	Path
Parent: 2,3-DMSA					
$C_6 H_{10} O_5$		162	0.00	22.8	Scheme 1 (Path A and Path B)
$C_5 H_8 O_3$		116	-0.40	9.2	Scheme 1 (Path A)
Parent: 2,2-DMSA					
$C_6 H_{10} O_5$		162	0.00	9.5	Scheme 2 (Path A and Path B)
$C_5 H_8 O_3$		116	-0.40	13.2	Scheme 2 (Path A)
$C_5 H_8 O_4$		132	0.00	6.0	Scheme 2 (Path A)
$C_5 H_8 O_5$		148	0.40	8.7	Scheme 2 (Path B)

529

530

531

532

533

534

535

536

537

538

539

540
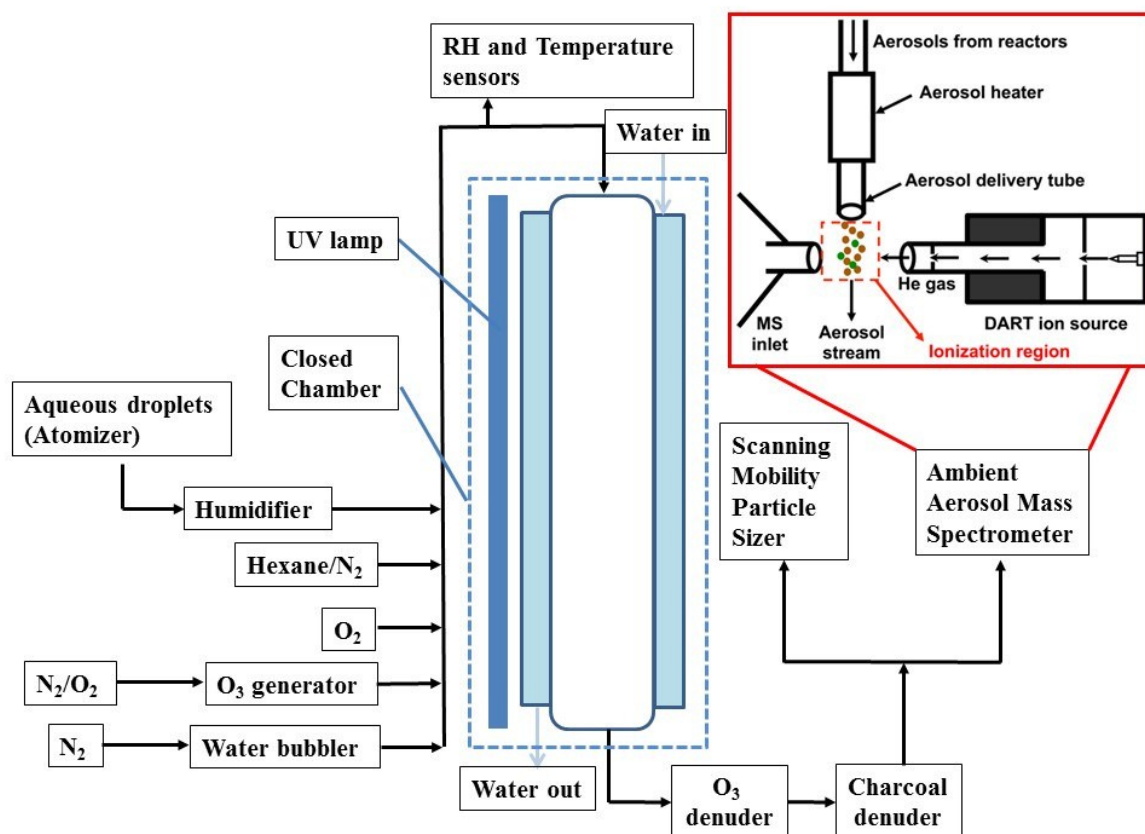
541 Fig. 1 Schematic diagram of an aerosol flow tube reactor coupled with an ambient aerosol mass

542 spectrometer for investigating the heterogeneous OH oxidation of aqueous DMSA droplets.

543
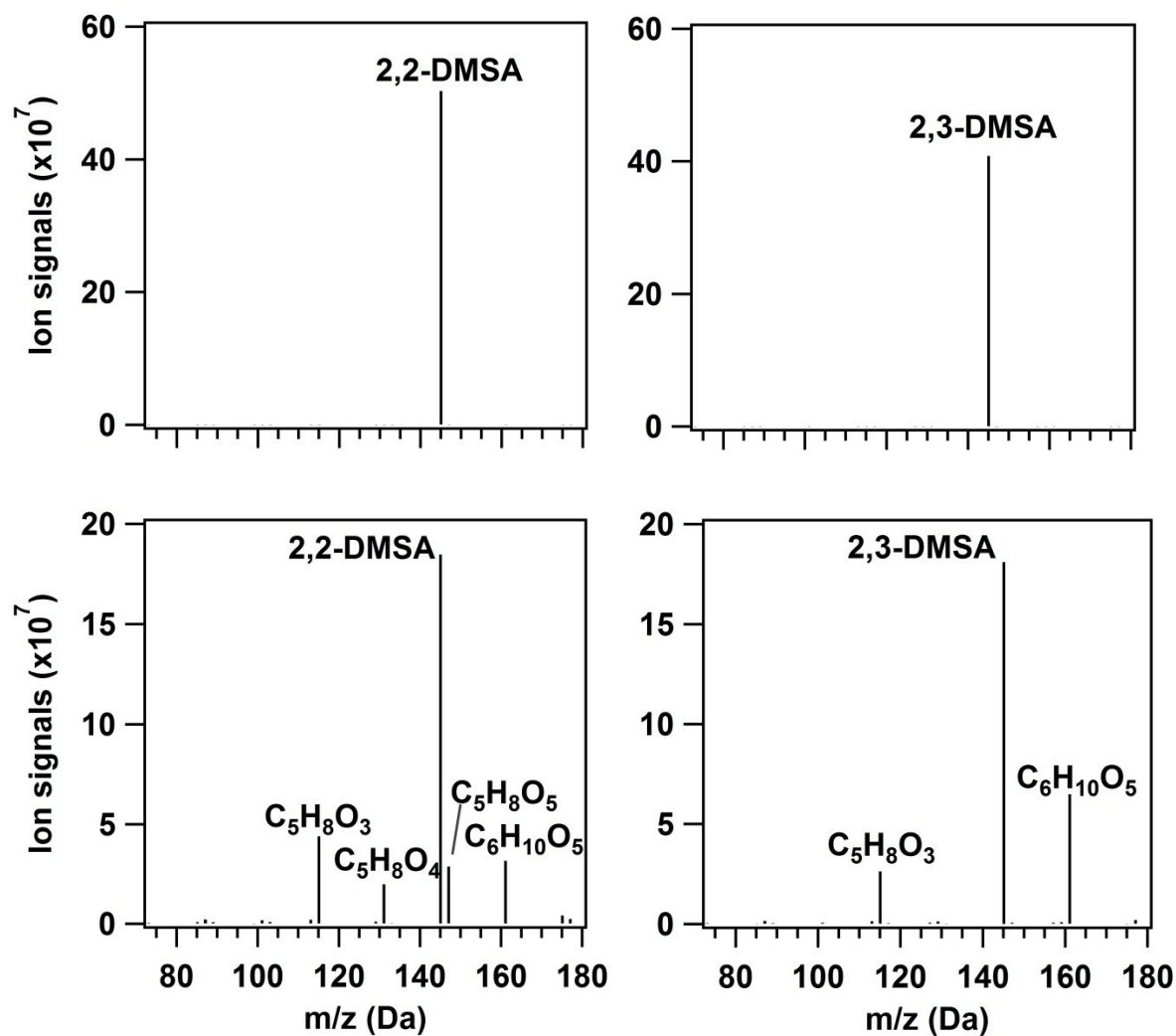
Fig. 2 Mass spectra of 2,2-DMSA (left panel) and 2,3-DMSA (right panel) before and after oxidation at about one oxidation lifetime (2,2-DMSA: lifetime of 1.04; 2,3-DMSA: lifetime of 1.23). One oxidation lifetime indicates that the parent has been decayed 1/e. Details of minor products can be found in the supporting information.
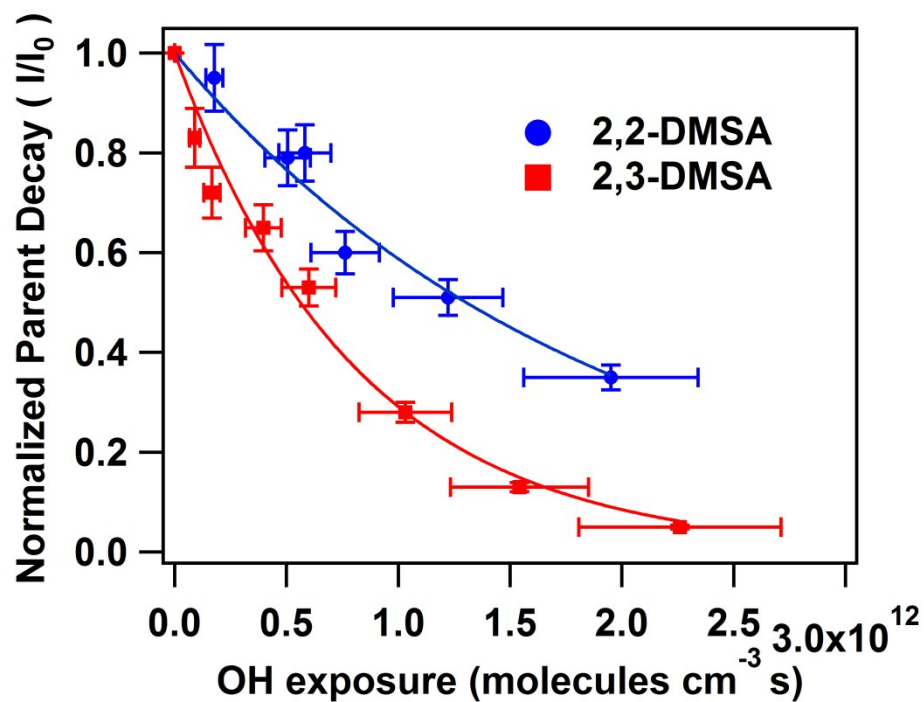
Fig. 3 Decay curves of the 2,2-DMSA and 2,3-DMSA. An exponential decay curve (solid line) is fitted for each curve to determine the OH reaction rate constant, k.

564

565
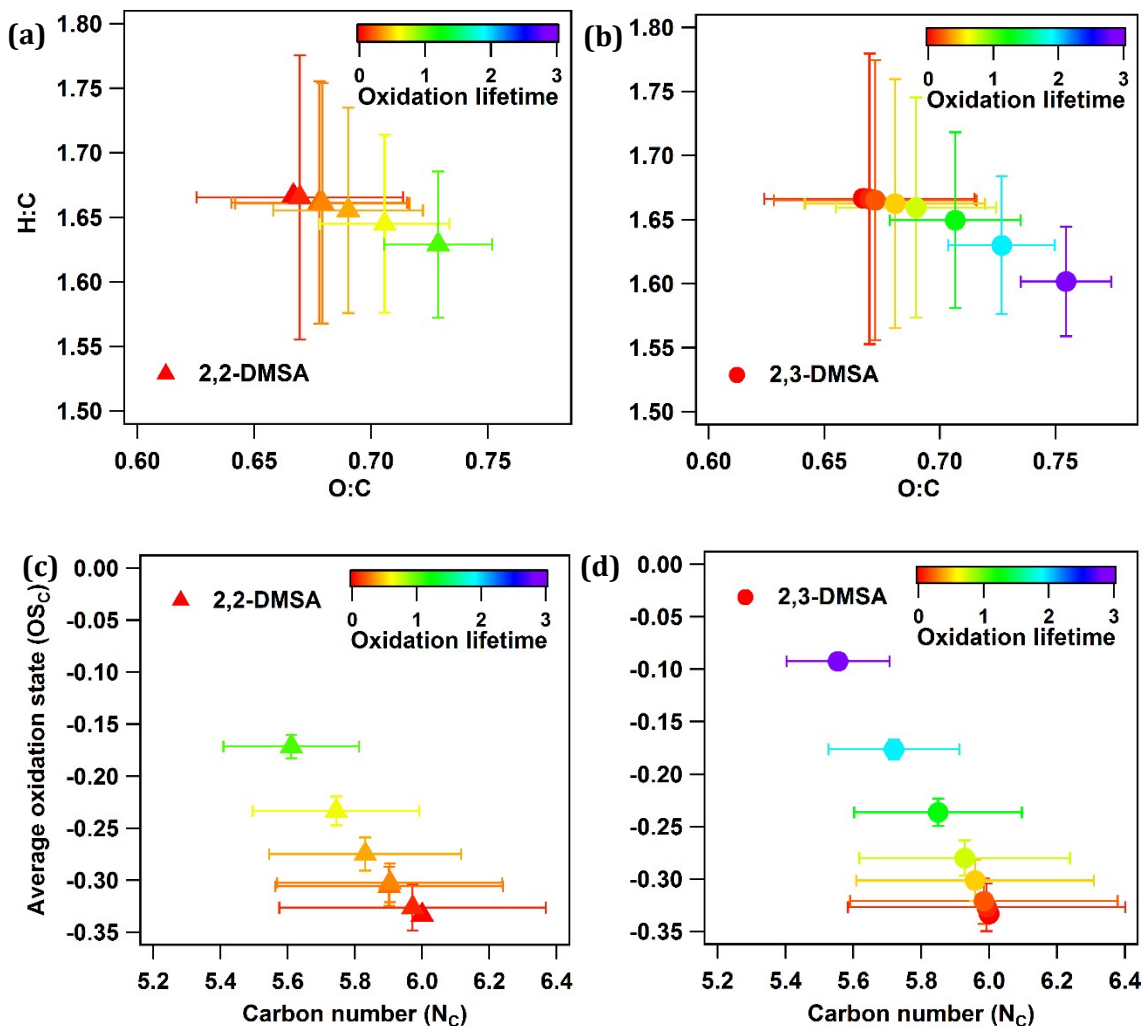
Fig. 4 (a, b) van Krevelen diagram shows the evolution of average *H/C* ratio and *O/C* ratio of

2,2-DMSA and 2,3-DMSA aerosol at different oxidation lifetime. (c, d) The evolution of average

carbon oxidation state ($OS_C = 2 \times (O/C) - (H/C)$) and average carbon number (N_C) of the 2,2-

DMSA and 2,3-DMSA aerosol at different oxidation lifetime. Oxidation lifetime is the OH
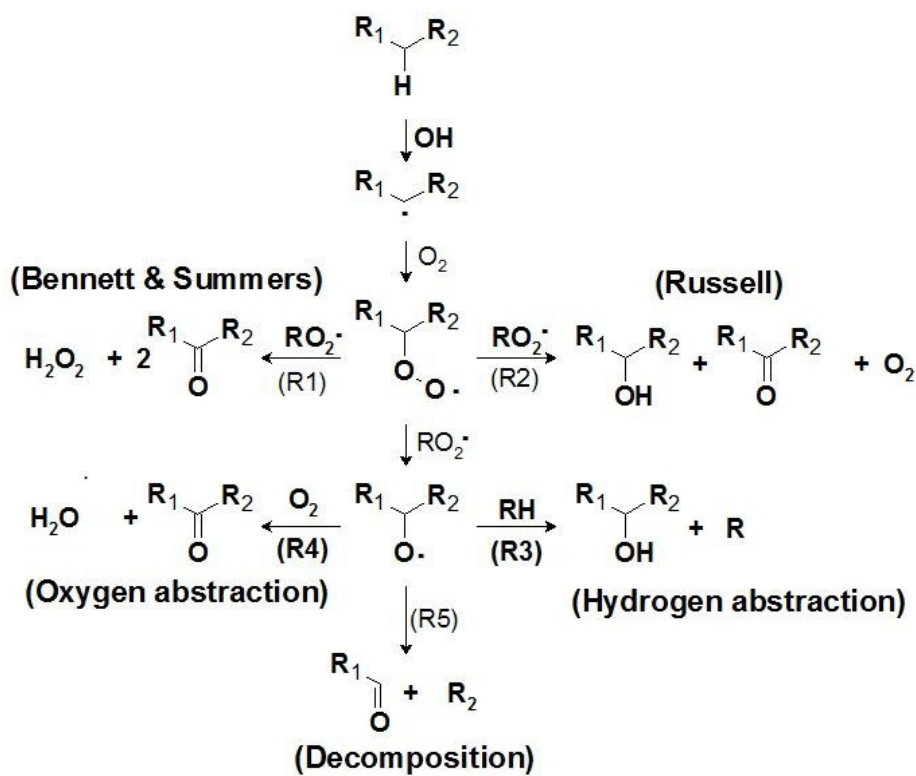
exposure is multiplied by the fitted OH rate constant, *k*.

571

572

573

574

575

576

577

578

579

580

581

582

583   Fig. 5 The general reaction scheme proposed to explain the formation of observed reaction

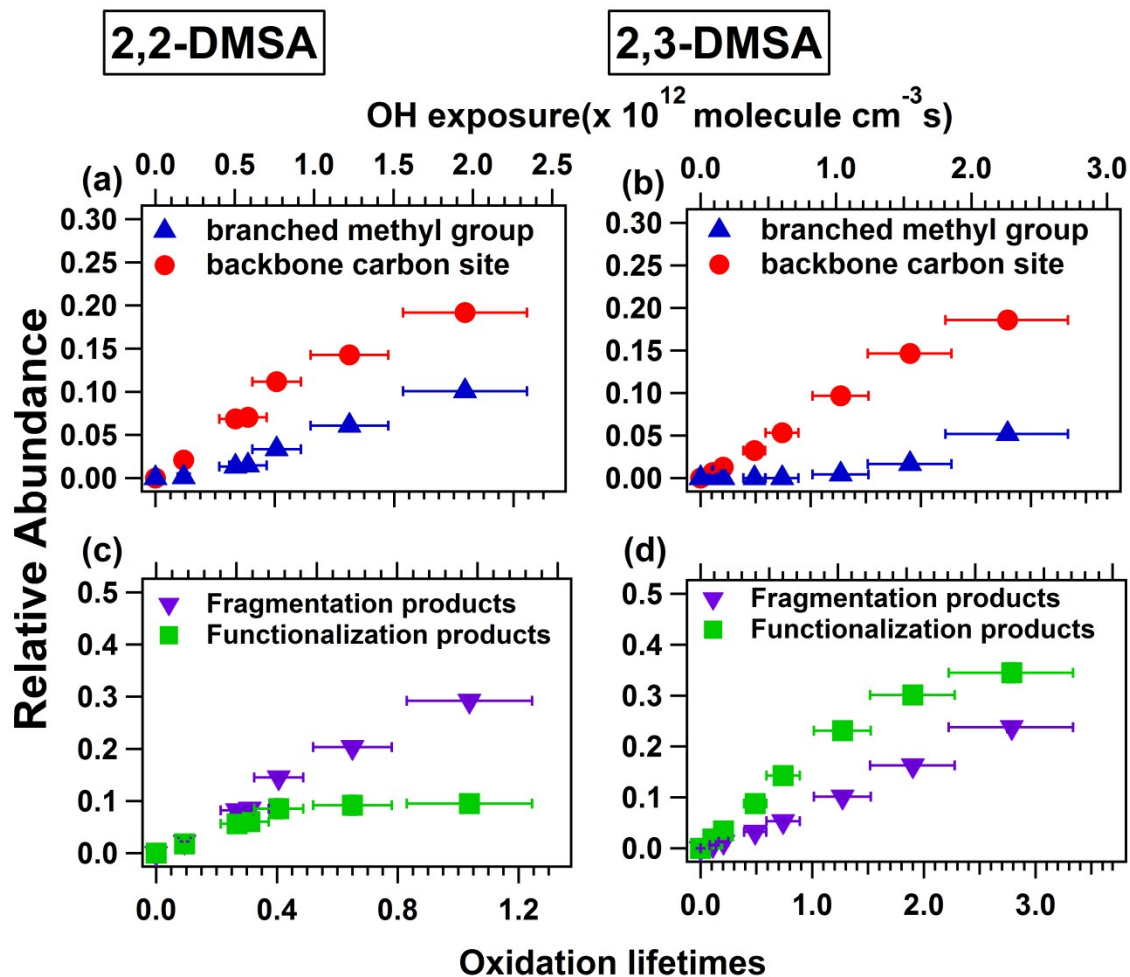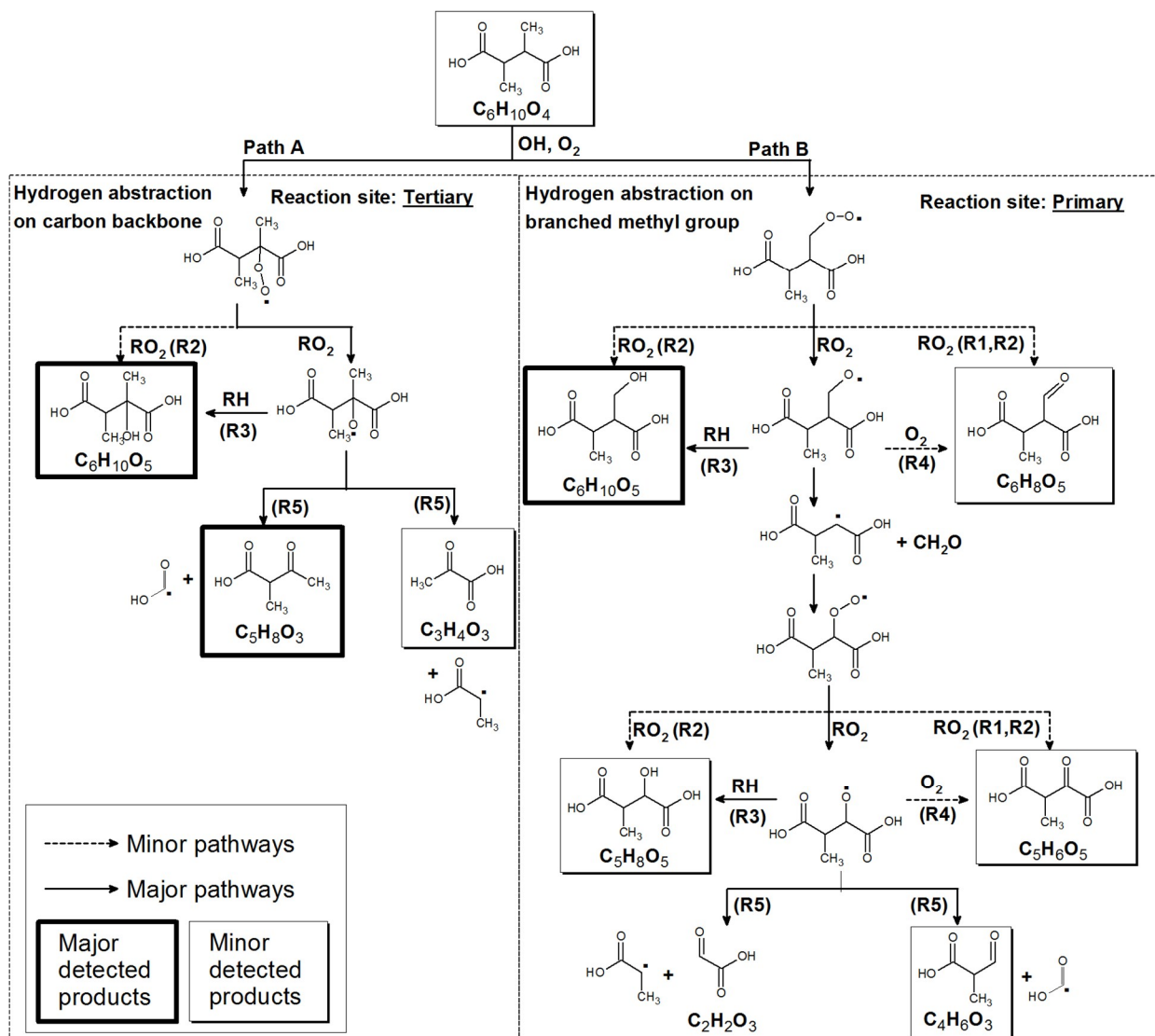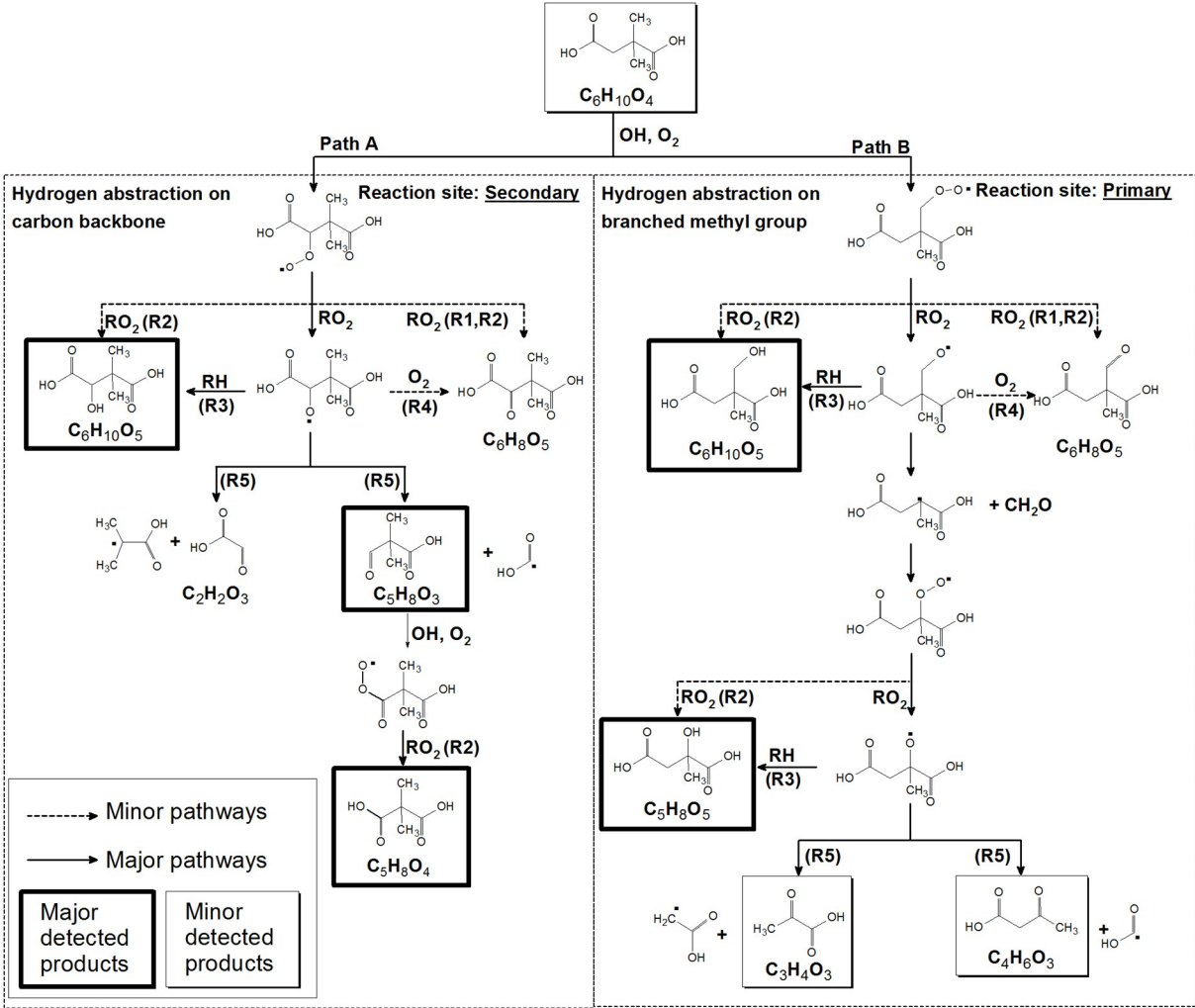584   products in the heterogeneous OH oxidation of 2,2-DMSA and 2,3-DMSA.

Fig. 6 Upper panel (a and b): The relative abundance of fragmentation products formed after the hydrogen abstraction occurred either on the backbone carbon site or branched methyl group; Lower panel (c and d): The relative abundance of functionalization products and fragmentation products resulted from the heterogeneous OH oxidation of 2,2-DMSA and 2,3-DMSA. Oxidation lifetime is the OH exposure is multiplied by the fitted OH rate constant, k. Note that only the proposed products in Schemes 1 and 2 are considered.

Scheme 1: Proposed reaction mechanisms for the heterogeneous OH oxidation of 2,3-dimethylsuccinic acid. The left dotted box highlights the hydrogen abstraction occurs on the backbone carbon site (Path A) and the right dotted box highlights the hydrogen abstraction occurs on the branched methyl group (Path B).

602

Scheme 2: Proposed reaction mechanisms for the heterogeneous OH oxidation of 2,2-dimethylsuccinic acid. The left dotted box highlights the hydrogen abstraction occurs on the backbone carbon site (Path A) and the right dotted box highlights the hydrogen abstraction occurs on the branched methyl group (Path B).

603